Abstract for the 38th Intl Workshop on Water Waves and Floating Bodies, 7th - 10th May, 2023, Michigan, AMERICA

Waves generated by a submerged ellipsoid when entering a lock

Yi-Han Liu, Guang-Wei Zhao, Zhi-Ming Yuan*

Dep. of Naval Architecture, Ocean & Marine Engineering, University of Strathclyde

E-mail Address of the presenting author: zhiming.yuan@strath.ac.uk

HIGHLIGHTS

- A piston mode of free surface motion is observed in the gap between the ellipsoid and lock gate
- The piston motion of free surface in the lock would significantly affect the force on the moving body. A negative wave-making resistance was observed when the ellipsoid was very close the lock gate.

1 INTRODUCTION

Due to a sudden change in waterways, such as bank or water depth changes, the hydrodynamics of a moving ship are complicated. The most typical and complex scenario of such manoeuvre is a ship enters a lock. Most of the published work are mainly focused on the manoeuvrability or the hydrodynamic force of the ship. For example, Vantorre and Richter (2011) found the hydrodynamic characteristics of the ship entering a lock would change with factors such as approach channel and structure layouts, water depth, translation waves, return flow, and cushion effects etc. In early years, the experimental measurements used to be the most reliable approach of this problem. Many experiments were conducted in the David Taylor Model Basin to study the effect of cross-sections on manoeuvrability (Schoenherr, 1960). More recently, the CFD (Tezdogan 2016) method and the 3D potential flow method (Xu, 2016) have also been applied to this problem. In these studies, the free surface was treated as a rigid wall and the waves in the lock were ignored. Yuan (2019) went a step further by including the free surface in his simulations, but the unsteady terms in the free surface boundary conditions were not considered.

In order to simulate the unsteady 3D waves in the lock, this paper keeps the unsteady terms in the free surface condition based on Yuan's work (2019) and introduces a three-level difference scheme to make the calculation results correlated at all time steps possible. An experiment was conducted on a submerged ellipsoid entering a lock. From the simulation and measurement results, it is found that there are waves propagating in front of the ship, creating a "piston" phenomenon in the gap between the ship bow and lock gate. As a consequence, oscillations in the wave field and wave making resistance are observed, and these oscillations are highly dependent on ship speed.

2 METHDOLOGY AND ECPERIMENT SETTINGS

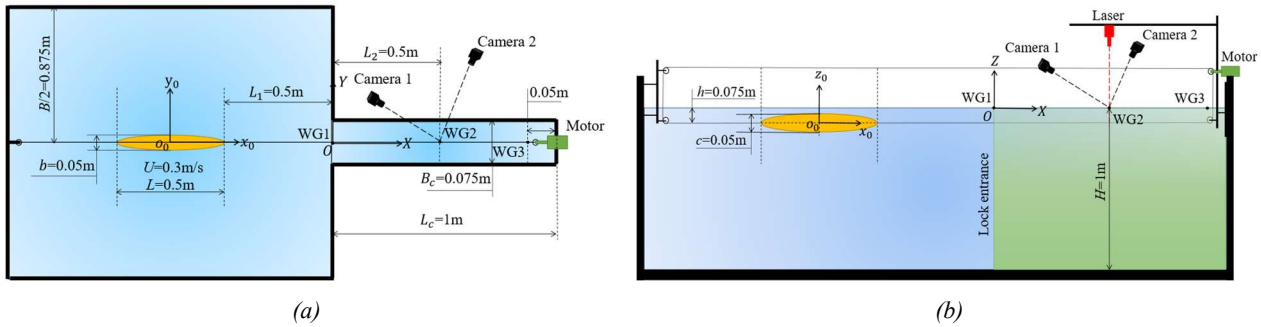

Figure 1. **The sketch of the problem and the experimental setup. (a) Top view. (b) Side view.**

Both experimental tests and numerical simulations are conducted to evaluate the hydrodynamics of a submerge ellipsoid when it enters into a narrow lock from open water, as shown in ***Figure 1.*** Two right-handed coordinate systems are used in the present study: a global coordinate system *O-XYZ* that is fixed to the middle of the lock entrance, and a local coordinate system o_0-$x_0y_0z_0$ which is located at the geometry centre of the ellipsoid. During the testing, the submerged ellipsoid is towed by a wire loop that connected to four pulleys in a rectangular configuration. Driven by a motor, the ellipsoid will enter the lock with a target forward/backward speed. At

the same time, a steady-state laser transmitter is used generate at an illuminant at the position where the wave elevation needs to be measured. During the process of entering the lock, the cameras set above the lock area will continuously film the light dot with a frequency of 60 Hz. Thus, the time-history information of the free surface elevation at this point is obtained by calculating the position of the light dot.

The numerical modelling is based on a 3D potential flow method. The fluid here is assumed to be inviscous and incompressible, and the flow is irrotational. A velocity potential *φ(x,y,z,t)* is used to descript the flow. The free surface is expressed by the dynamics and kinematics free surface conditions. In order to investigate the unsteady effect, the unsteady terms in the free surface condition are kept, while the nonlinear terms are ignored. The linearized unsteady kinematic and dynamic free surface condition under the body-fixed coordinate system can be written as:

$$\zeta_t - u\zeta_x - \varphi_z = 0, \text{ on } z = \zeta \tag{1}$$

$$\varphi_t + g\zeta - u\varphi_x + \frac{1}{2}\left[(\varphi_x \cdot \varphi_x) + (\varphi_y \cdot \varphi_y) + (\varphi_z \cdot \varphi_z)\right] = 0, \text{ on } z = \zeta \tag{2}$$

Here $\zeta(x, y, t)$ represents the wave elevation and g is the gravitational acceleration. The above two conditions are satisfied at $z = \zeta$. The free surface conditions are discretized by using a three-level differential scheme:

$$(\varphi_t)_{i,j}^n = \frac{1}{\Delta t}\left(\frac{3}{2}\varphi_{i,j}^n - 2\varphi_{i,j}^{n-1} + \frac{1}{2}\varphi_{i,j}^{n-2}\right), \quad (\varphi_x)_{i,j}^n = \frac{1}{\Delta x}\left(\frac{3}{2}\varphi_{i,j}^n - 2\varphi_{i,j+1}^n + \frac{1}{2}\varphi_{i,j+2}^n\right) \tag{3}$$

$$(\zeta_t)_{i,j}^n = \frac{1}{\Delta t}\left(\frac{3}{2}\zeta_{i,j}^n - 2\zeta_{i,j}^{n-1} + \frac{1}{2}\zeta_{i,j}^{n-2}\right), \quad (\zeta_x)_{i,j}^n = \frac{1}{\Delta x}\left(\frac{3}{2}\zeta_{i,j}^n - 2\zeta_{i,j+1}^n + \frac{1}{2}\zeta_{i,j+2}^n\right) \tag{4}$$

Based on the above equations, an iterative algorithm is applied to the boundary value problem. The steady solutions on the first two time steps are used as the initial values of φ and ζ. The kinetic condition is then solved firstly to obtain a solution for ζ at the new time step and this solution will be substituted into the dynamic condition to obtain the source density and the corresponding velocity potential φ. At this point, an iterative calculation of the current time step is completed. At each iterative step k, Eq. (1) and (2) can be respectively expressed as below:

$$\frac{1}{\Delta t}\left(\frac{3}{2}\zeta_{i,j}^{(n,k)} - 2\zeta_{i,j}^{(n-1,k)} + \frac{1}{2}\zeta_{i,j}^{(n-2,k)}\right) - U\frac{1}{\Delta x}\left(\frac{3}{2}\zeta_{i,j}^{(n,k)} - 2\zeta_{i,j+1}^{(n,k)} + \frac{1}{2}\zeta_{i,j+2}^{(n,k)}\right) - \frac{\partial\varphi_{i,j}^{(n+1)}}{\partial z} = 0 \tag{5a}$$

$$\frac{3}{2}\left(\frac{1}{\Delta t} - \frac{U}{\Delta x}\right)\zeta_{i,j}^{(n,k)} + 2\frac{U}{\Delta x}\zeta_{i,j+1}^{(n,k)} - \frac{1}{2}\frac{U}{\Delta x}\zeta_{i,j+2}^{(n,k)} = \frac{2}{\Delta t}\zeta_{i,j}^{(n-1,k)} - \frac{1}{2}\frac{1}{\Delta t}\zeta_{i,j}^{(n-2,k)} + \frac{\partial\varphi_{i,j}^{(n,k)}}{\partial z} \tag{5b}$$

$$\frac{1}{\Delta t}\left(\frac{3}{2}\varphi_{i,j}^{(n,k)} - 2\varphi_{i,j}^{(n-1,k)} + \frac{1}{2}\varphi_{i,j}^{(n-2,k)}\right) - U\frac{\partial\varphi_{i,j}^{(n,k)}}{\partial x} + g\zeta_{i,j}^{(n,k)} = 0 \tag{6a}$$

$$\frac{3}{2}\frac{1}{\Delta t}\varphi_{i,j}^{(n,k)} - U\frac{\partial\varphi_{i,j}^{(n,k)}}{\partial x} = \frac{2}{\Delta t}\varphi_{i,j}^{(n-1,k)} - \frac{1}{2}\frac{1}{\Delta t}\varphi_{i,j}^{(n-2,k)} - g\zeta_{i,j}^{(n,k)} \tag{6b}$$

After the above calculation, $\varphi_{i,j}^{(n,k)}$ and $\zeta_{i,j}^{(n,k)}$ are predicted as the new value of $\varphi_{i,j}^n$ and $\zeta_{i,j}^n$. In order to generate a stable result, these new values must satisfy both conditions of $\left|\varphi_{i,j}^{(n,k)} - \varphi_{i,j}^{(n,k-1)}\right| < \epsilon$ and $\left|\zeta_{i,j}^{(n,k)} - \zeta_{i,j}^{(n,k-1)}\right| < \epsilon$ before proceeding to the next time step.

A Rankine source panel code developed at Strathclyde University, namely MHydro, is used to solve the boundary value problem. After the unknown potential φ has been solved, the forces/moments can be obtained from the nonlinearized Bernoulli's equation

$$F_i = \iint_S Pn_i ds = \iint_S \{-\rho[\varphi_t - U\varphi_x + \frac{1}{2}(\varphi_x^2 + \varphi_y^2 + \varphi_z^2)]\}n_i ds, i = 1, 2, \ldots, 6 \tag{7}$$

Similarly, the free surface elevation can be expressed as:

$$\zeta(x, y, t) = -\frac{1}{g}\left[\varphi_t - U\varphi_x + \frac{1}{2}(\varphi_x^2 + \varphi_y^2 + \varphi_z^2)\right] \tag{8}$$

3 RESULTS AND DISCUSSIONS

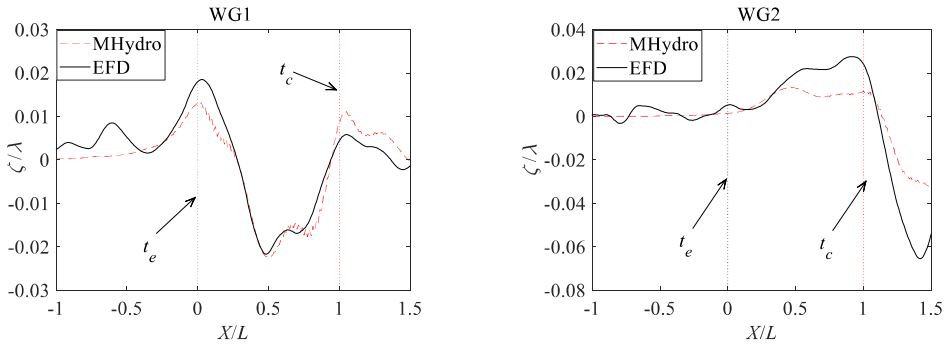

(a) *(b)*

Figure 2. **Validation of free surface elevations at F_r=0.136. t_e is the moment when the bow of the ellipsoid reaches the lock entrance and t_c is the moment when the ellipsoid is completely in the lock. X is the position of the ellipsoid bow under the global coordinate system. (a) Free surface elevation at WG1; (b) free surface elevation at WG2.**

Firstly, a validation is conducted by comparing the numerical results with the experimental measurement. As shown in ***Figure 2***, the free surface elevations at two wave gauges are captured by both numerical (MHydro) and experimental (EFD) methods. The agreement of these two methods is generally satisfactory. Some oscillations are captured by the measurements before the ellipsoid enters the lock (X/L<0). These oscillations are likely to be initiated at the acceleration stage. While in the numerical simulation, a constant speed U is given at the first time step of simulation. Therefore, these oscillations are not observed in the numerical results. It is also found that the numerical predictions at WG2 is less satisfactory, particularly when the bow is getting closer to the lock gate, indicating some nonlinear phenomenon occurs when the gap between lock gate and ellipsoid is small.

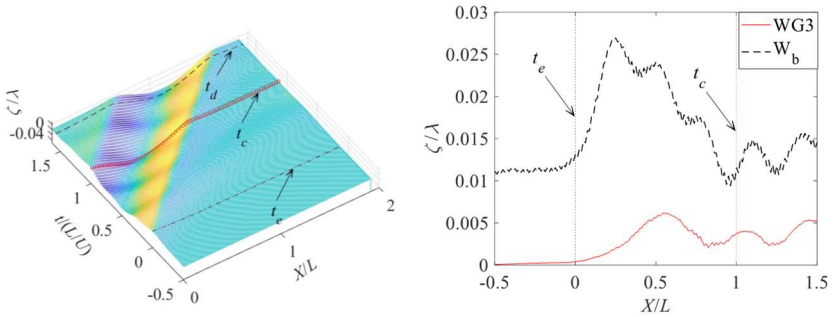

(a) *(b)*

Figure 3. **Waves evolution during the ellipsoid entering the lock at F_r=0.136. (a) Waterfall plot of wave cut in the centre line of lock; (b) free surface elevation at WG3 and the ellipsoid bow.**

Wave Gauge 3 (WG3) is used to record the time history of the waves at the lock gate when the ellipsoid is entering the lock. It is also interesting to monitor the wave elevation at the ellipsoid bow in the body-fixed coordinate system, as shown in ***Figure 3*****(b)**. The evolution of the waves in the centre line of lock is shown in ***Figure 3*****(a)**. After the ellipsoid bow reaches the lock entry, the waves in the lock are quickly built. It reaches its maximum value when half of the ellipsoid is in the lock (X/L=0.5). As the ellipsoid keeps entering the lock, some oscillations are observed at WG3. These wave-like oscillations will interact with the bow waves, causing oscillations of free surface elevation. It should be noted that the bow waves are local waves moving at the same speed of the ellipsoid. However, the free surface in the lock is more like a piston, which rises and falls globally in the gap between the ellipsoid and the lock gate. This piston mode of free surface motion can only be observed when the lock gate is closed. As the ellipsoid enters the lock, the water in the lock cannot quickly evacuate from the lock. The existence of the lock gate stops the accelerated water particles keeping moving forward. The kinetic energy is converted into gravitational energy, causing a rising of free-surface. As the free surface rises to a certain level, the accumulated potential energy will release to generate a return flow in the channel, and the free surface elevation is lowered. The piston motion in the gap is a process of energy conversion, and

we can take the free surface as a vertical spring. During the entering process, the gap is getting smaller, and the restoring coefficient of the spring reduces gradually.

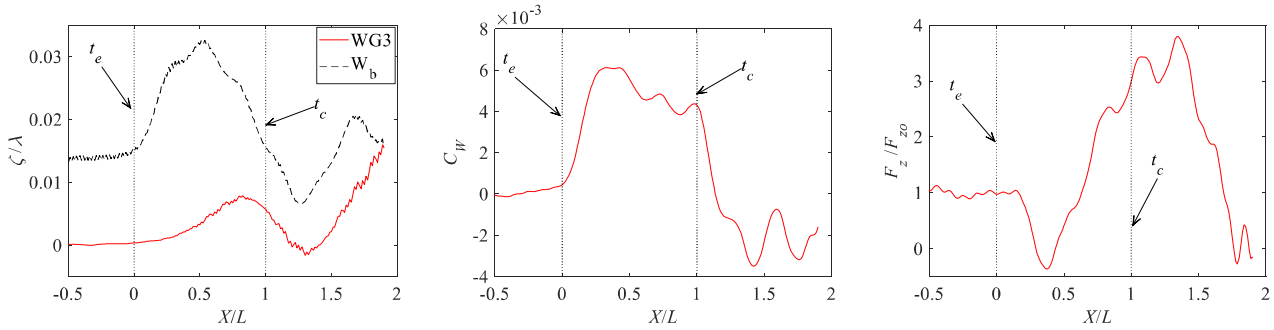

Figure 4. **Free surface elevation and forces on the ellipsoid when it enters the lock at F_r=0.2. (a) Free surface elevation at WG3 and the bow; (b) wave-making resistance coefficient; (c) Vertical force nondimensionalized by the force at open water.**

Obviously, the piston motion in the lock is affected by the entering speed. As can be seen from ***Figure 4*** **(a)**, only one trough is observed at WG3 when the speed increases to F_r=0.2, and the amplitude of the motion is getting larger. The wave-making resistance increases quickly after the bow enters the lock, as shown in ***Figure 4*** **(b)**. It reaches its maximum value at X/L=0.5, after which a decrease is expected. However, a high resistance is sustained until X/L=1. This is due to the rising of free surface (or piston) at the front of the ellipsoid, which makes the bow pressure higher. Because of the piston effect, the free surface starts to fall after X/L=1. It creates a low pressure field in the lock, sucking the ellipsoid to move towards the lock. That is why we observe a negative wave-making resistance after the ellipsoid is completely in the lock. As the free surface is lowered, the water is the lock evacuates quickly to wake, creating a crest in the stern area. The piston-like free surface then rises again in the lock when the bow gets very close to the lock gate. It increases the pressure at the bow. But the pressure at the stern is still in a high level, and the resistance remains negative.

Another interesting finding is the vertical force. After the ellipsoid enters the lock, a surprising drop of F_z is observed, as shown in ***Figure 4*** **(c)**. This is because the rising free surface in the lock inhales water. The water under the ellipsoid moves forward under the global coordinate system. It's like the moving speed of the ellipsoid is getting lower. The piston (free surface) then moves down and creates a returning flow at the bottom, which accelerates the entering speed. As a results, the vertical force increases. When the free surface starts to rise again, the vertical force falls.

REFERENCES

Schoenherr, K. (1960). "Data for estimating bank suction effects in restricted water and on merchant ship hulls", David Taylor Model Basin Report.

Tezdogan, T., et al. (2016). "A numerical investigation of the squat and resistance of ships advancing through a canal using CFD." Journal of marine science and technology **21**(1), 86-101.

Vantorre, M., et al. (2011). "Maneuverability in lock access channels." What's new in the design of navigation locks 2nd International Workshop, PIANC–New Orleans, 13-14.

Xu, H., et al. (2016). "Unsteady hydrodynamic interaction between two cylindroids in shallow water based on high-order panel method." Engineering Analysis with Boundary Elements **70**, 134-146.

Yuan, Z. M. (2019). " Ship Hydrodynamics in Confined Waterways." Journal of Ship Research **63**(1): 16-29.